Fixed-frequency beam-scanning antenna with a reconfigurable metasurface

Journal of Ultrafine Grained and Nanostructured Materials
https://jufgnsm.ut.ac.ir
Vol. 58, No.1, June 2025, pp. 45-54
Print ISSN: 2423-6845 Online ISSN: 2423-6837
DOI: 10.22059/jufgnsm.2025.01.05

Effect of In-Situ Alloying with Si on the Microstructure of a Novel Ti-5Cu Alloy Manufactured by Laser Powder Bed Fusion

M. Talebi [1], A. Razaghian[1*], B. Niroumand[2], A. Saboori[3]

[1]Department of Materials Engineering, Imam Khomeini International University (IKIU), Qazvin, 3414896818, Iran
[2]Department of Materials Engineering, Isfahan University of Technology (IUT), Isfahan, 8415683111, Iran
[3]Department of Management and Production Engineering, Politecnico di Torino, Torino, 10129, Italy

Recieved: 11 April 2025; Accepted: 24 April 2025

[*]Corresponding author, E-mail: razaghian@eng.ikiu.ac.ir

ABSTRACT

The present work aims to explore the influence of Si addition on the microstructure of a novel Ti-5Cu alloy produced by the Laser Powder Bed Fusion (L-PBF) technique, under an in-situ alloying strategy. For this purpose, Ti–5Cu and Ti–5Cu–1Si samples were manufactured under the same volumetric energy density (VED), i.e., 50.26 J/mm³. The findings revealed that incorporating 1 wt% Si into the Ti-5Cu alloy converted the prior β columnar and equiaxed grains with an average size of 41 μm and 22 μm, respectively, to finer equiaxed prior β grains within the Ti-5Cu-1Si microstructure, which featured with an average size of about 8 μm. Greater tendency for columnar to equiaxed transition and a notable grain refinement with Si addition were linked to a greater constitutional supercooling zone created by the rejection of Si solute atoms in front of the solidification front. Comparison of the solidification ranges for Ti-5wt%Cu and Ti-1wt%Si alloys plotted by PANDAT software revealed that Si has a more severe impact on the solidification range than Cu, making it a potentially better option for inducing columnar to equiaxed transition. Incorporating 1% Si to the Ti-5Cu alloy increased the growth restriction factor from 35 to 60 K, resulting in an almost 3-fold reduction in grain size. Addition of Si to the Ti-5Cu alloy also significantly refined the average length of α lath from about 4 μm to about 1.7 μm in the microstructure of Ti–Cu–Si alloys.

Keywords: *Additive Manufacturing, Laser Powder Bed Fusion, Ti-5Cu-1Si alloy, Columnar to Equiaxed Transition, Growth Restriction Factor.*

1. Introduction

Additive manufacturing (AM), often known as three-dimensional (3D) printing, is a novel manufacturing technology that involves making items layer by layer utilizing a computer model and a methodology capable of constructing components with near-net shape [1-4]. This technology challenges the supremacy of traditional manufacturing processes, such as subtractive procedures, by producing extremely complex metallic or metallic matrix composites/nano-composites products with minimal material waste [3,4]. Fusion-based AM of metallic objects can be accomplished using directed energy deposition (DED) [5] or powder bed fusion (PBF) techniques [3]. In PBF processes, selective melting of a thin layer of metal powder previously spread on a platform can be accomplished by a focused heat source such as a laser or an electron beam. Laser powder bed fusion (L-PBF) and electron beam powder bed fusion (EB-PBF) are the two main technologies of PBF group, which are generally quite different in terms of their heating source, power density, and energy/material transfer principles [6-8].

In recent years, much of the research into metal AM technologies has focused on preventing the

formation of columnar grains, particularly in Ti-based alloys, which result in anisotropic mechanical properties and are, therefore, perceived to be undesirable and present challenges in component design [6,9-13]. The steep thermal gradient, combined with a scarcity of nucleation events ahead of the solid/liquid (S/L) interface, favors epitaxial growth of β grains, which is typically the governing growth mechanism during L-PBF processing of Ti alloys [9,6,14]. Multiple strategies have been proposed to tackle this challenge by creating a high constitutional supercooling (ΔT_{CS}) zone, which aims to overcome this steep thermal gradient and, hence, regulate the final microstructure [6,12,14]. One of them entails adjusting process parameters such as laser power and scanning speed to establish a judicious control of the heat input, which in turn will optimize thermal gradient (G) and solidification rate (R) of the solidification front, facilitating the columnar to equiaxed transition (CET) phenomenon [2,8].

In addition to process parameters, the influence of introducing elements that can generate a large ΔT_{CS} region in front of the solidification front is regarded as a key solution from the aspect of inducing the CET phenomenon [6,9-13]. According to Talebi et al. [6], the CET phenomena in L-PBFed Ti-5Cu alloy is primarily caused by the uniform distribution of Cu, reduced G owing to increased volumetric energy density (VED), and high ΔT_{CS} capacity of Cu. Mosallanejad et al. [12] achieved a fine-grained fully equiaxed structure in EBM processing of Ti6Al4V-7Cu alloy due to rather low G of the EBM process combined with the high capacity of Cu in inducing ΔT_{CS} in front of the columnar prior β- grains.

AM in-situ alloying of Ti-based alloys alleviates concerns regarding the powder-based AM methods by reducing the restrictions of using pre-alloyed powders, such as narrow composition range, limited availability, and cost [15]. However, achieving a dense and homogeneous material necessitates meticulous selection of elemental powder sizes and process parameters, informed by their physical and thermo-physical characteristics [15-19]. A previous study [16] demonstrated that the feasibility of in situ Ti-5 wt.% Cu alloys produced via the L-PBF process is contingent upon utilizing a powder blend of Ti and Cu with the average particle diameter of approximately 30 μm and 7 μm, respectively, and under a high VED (77.55 J/mm^3). In fact, the larger size of Ti particles than the Cu particles is in accordance with lower laser absorption coefficient (0.1 [20]) and higher thermal conductivity of Cu (330 W/m.k [21]) than those of Ti (0.56, 31 W/m.k [20,21]), as well as the higher melting point of Ti (1940K) with regard to Cu (1357K).

In-situ alloying of the Ti–Cu-based alloys by L-PBF are mainly developed for biomedical applications [17-19, 22-24]. Nonetheless, undesirable phases such as columnar prior β grains and non-equilibrium acicular α› phase are still reported in the microstructure of L-PBFed Ti-5Cu alloy because of the high intrinsic cooling rates (10^3-10^8 K/s) and G (~10^{5-6} K/m) associated with the L-PBF process [6, 25,26]. On the other hand, considering the difference in physical and thermo physical properties of Cu and Ti elements, in-situ alloying of LPBFed Ti–Cu-based alloys under non-optimized process parameters will often result in inhomogeneous microstructures [15-19]. These occurrences can result in degraded mechanical and corrosion properties, making it challenging for LPBFed Ti–Cu-based alloys to meet application requirements.

Therefore, through post-processing operations, some efforts have been made to eliminate undesirable microstructures and chemical inhomogeneity of L-PBFed Ti–Cu-based alloys [23,25, 27-28]. Talebi et al. [28] found that heating in-situ L-PBFed Ti-5Cu alloy to 1050 °C resulted in the dissolution of all columnar β grains, full solubility of the non-dissolution zone of Cu and Ti, and elimination of the acicular α› phase in the as-built microstructure. This was followed by the development of fully equiaxed prior-β grains, enhanced homogeneity, and the production of the equilibrium lath-like α phase in the microstructure of the heat-treated Ti-5Cu alloy. However, post-processing operations are costly and time-consuming, and in certain circumstances, create unwanted microstructures that deteriorates the properties.

The main objective of this study is to investigate the impact of Si addition on the solidification microstructure, explicitly focusing on the CET phenomenon in the microstructure of LPBFed Ti–5Cu alloy. Additionally, it assesses the feasibility of in-situ alloying of LPBFed Ti–5Cu–1Si from the perspective of microstructural homogeneity.

2. Experiments

2.1 Materials and manufacturing method

The powders used for manufacturing L-PBFed Ti-5Cu and L-PBFed Ti-5Cu-1Si samples include commercially pure Ti (grade 1, ≤50 μm, LPW, UK), commercially pure Cu powder (≤20 μm, Sandvik Osprey Ltd.) and commercially pure Si (≤1 μm). L-PBFed samples were built by a Concept Laser Mlab Cusing-R machine equipped with a 100 W fiber laser and a spot size of around 50 μm. As shown in Fig. 1a, cubic 1×1×1 cm^3 L-PBFed Ti-5Cu and L-PBFed Ti-5Cu-1Si samples were printed on a Ti substrate under VEDs of 50.26 J/mm^3. Fig. 1a shows the moment of printing samples

on the L-PBF-machine platform. The scanning strategy was striping form with 67° rotations, and a distributed layer thickness of 25 μm was used to print all the samples. After printing, the samples were removed from the Ti substrate and halved along the build direction using a micro cutter for microstructural analyses on Y-Z surfaces (Fig. 1b).

The microstructural evaluation was carried out by the standard metallographic techniques and using Kroll's reagent (1wt. % HF, 4wt. % HNO_3 and 95wt. % H_2O). Optical microscopy (OM, Olympus-BX-51M), scanning electron microscopy (SEM, Philips XL30) and field emission electron microscopy (FE-SEM, Quanta Feg 450) equipped with energy dispersive spectroscopy (EDS) instrument were carried out on the resulting Y-Z surfaces (Fig. 1b). Phase analysis was conducted using X-ray Diffraction analyses (XRD, Asenware -AW-XDM300, and Cu-Kα radiation), incorporating a step time of 1s and step size of 0.1°. PANalytical X'Pert, HighScore Plus software was employed for phase detection and profile fitting related to XRD patterns of L-PBFed Ti-5Cu-1Si sample. Pandat software was employed to plot non-equilibrium Scheil diagrams of the freezing ranges and to calculate the corresponding growth restriction factors (Q). Columnar and equiaxed prior β- grains size were measured by the linear intercept technique.

3. Results and discussions

3.1 Effect of Si addition on L-PBFed Ti-5Cu microstructure

Unlike the microstructure of L-PBFed CP-Ti samples characterized by columnar grains in previous literature [6, 28], the optical microstructure of L-PBFed Ti-5Cu alloy featured 22 μm average-sized equiaxed prior β-grains (Fig. 2a). This columnar-to-equiaxed transition stems from the high potency of Cu solute atoms in developing the ΔT_{CS} zone in front of columnar prior β-grains and the subsequent nucleation of equiaxed grains [6, 9,10,12,29]. Eq. (1) defines the growth restriction factor (Q) as the rate at which a solute element induces ΔT_{CS} in binary alloy systems [2].

$$Q = mC_0 (1 - k_0) \quad (1)$$

Where m is the slope of the liquidus line, C_0 is the solute content in the alloy melt, and k_0 is the corresponding equilibrium solute partition coefficient.

The Q values fluctuated based on the Schmidt-Fetzer and Kezlov method [30], revealing a Q factor of approximately 35 K for the Ti-5Cu alloy. As illustrated in Fig. 2a, large columnar prior β- grains still exist in the microstructure of the L-PBFed Ti-5Cu alloy sample, which have not been entirely mitigated by a pile-up of Cu atoms or partially transformed into equiaxed prior β-grains.

Compared to the L-PBFed Ti-5Cu alloy, the microstructure of the L-PBFed Ti-5Cu-1Si alloy revealed a fascinating array of smaller, equiaxed prior β-grains. The L-PBFed Ti-5Cu-1Si sample, is featured with 7.6 μm sized equiaxed prior β-grains (Fig. 2b). Conversely, as seen in Fig. 2c, the incorporation of Si has successfully inhibited the formation of the large columnar prior β-grains in the microstructure of the L-PBFed Ti-5Cu-1Si alloy sample, leading to thinner and shorter columnar prior β-grains. This results from the high potential of Si in generating ΔT_{CS} in front of columnar grains, which facilitates an effective CET phenomena in the microstructure of the L-PBFed Ti-5Cu-1Si alloy [31]. The incorporation of Si into the L-PBFed Ti-5Cu alloy results in a substantial Q of around 60 K, which is thought to significantly influence the grain refinement of the L-PBFed Ti-5Cu-1Si alloy.

Fig. 3 illustrates a direct correlation between

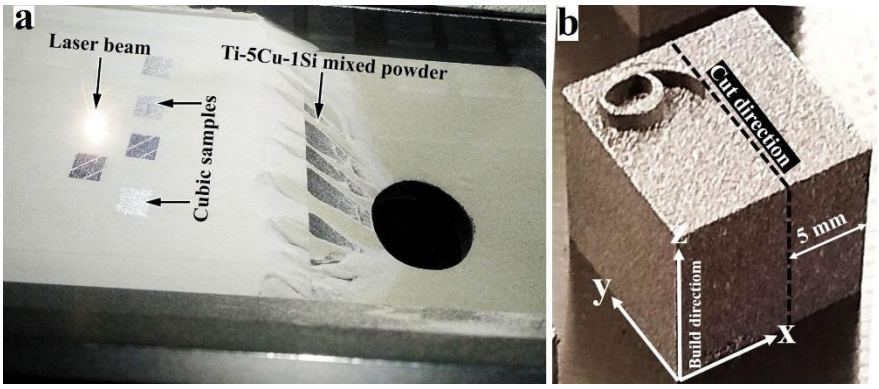

Fig. 1- a) Illustration of L-PBF-machine platform on which various samples are being printed and b) macrograph of a printed cube sample along with the cut direction in this work.

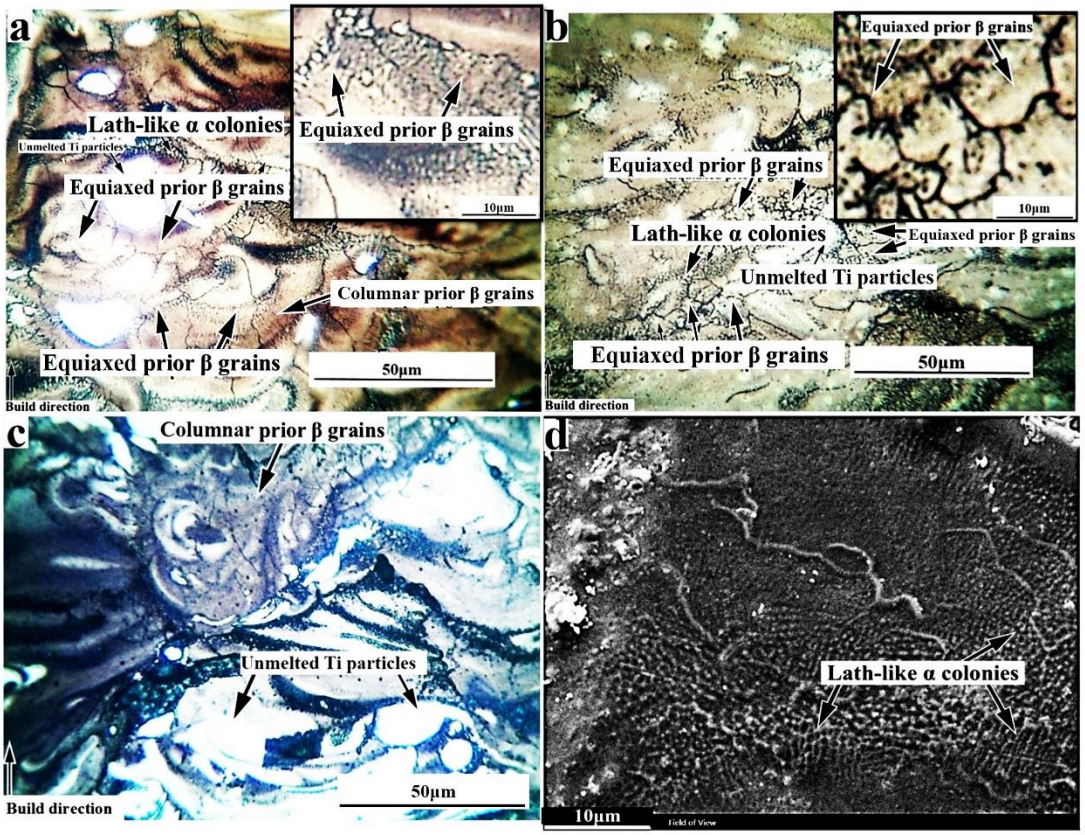

Fig. 2- OM micrographs from a) L-PBFed Ti-5Cu sample, b,c) L-PBFed Ti-5Cu-1Si sample and d) SEM micrograph of L-PBFed Ti-5Cu-1Si sample.

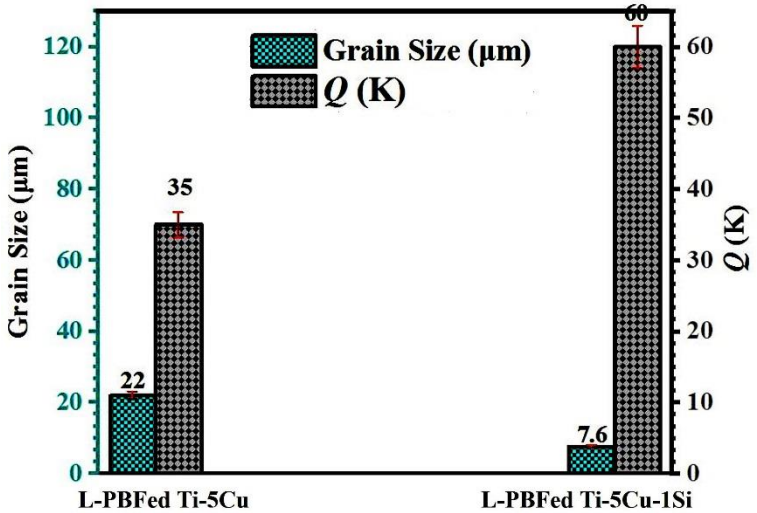

Fig. 3- Grain size evolutions depending on Growth restriction factor (Q) for the L-PBFed Ti-5Cu, and the L-PBFed Ti-5Cu-Si samples.

variations in Q and grain size across all samples, indicating that an increase in the Q value from 35 to 60 K corresponds to a reduction in average grain size of around 15 μm.

3.2 Effect of Cu and Si addition on freezing range

Welk et al. [32] employed a simple but effective approach to evaluate the influence of several alloying elements on the freezing range to determine the efficiency of each of these components in increasing the likelihood to induce CET in pure titanium. After analyzing various outcomes, it appears that employing CALPHAD-predicted phase diagrams for Ti-Ni, Ti-Fe, and Ti-Mo alloys is a beneficial method to assess whether the expansion of freezing ranges due to the inclusion of these elements is directly linked to the initiation of CET [32]. The influence of Si and Cu on the solidification range was examined using a CALPHAD method. Fig. 4a and 4b display the CALPHAD forecasts regarding alterations in the solidification range for Ti-5wt%Cu and Ti-1wt%Si alloys. Incorporating any of these elements expands the solidification range. Therefore, these elements can be viewed as promising contenders for enhancing the tendency for CET. When comparing the alterations in the solidification range between Ti-5wt%Cu and Ti-1wt%Si alloys, as shown in Fig. 4, it becomes evident that Si notably expands the solidification range. Therefore, Si can exert a more substantial influence on the CET compared to Cu.

3.3 Effect of Si on dimensions of lath-like α phase

As shown in Fig. 3a, Cu significantly alters the size of lath-like α phase in the L-PBFed Ti-5Cu microstructure and their size is limited to the interior space of the equiaxed prior β- grains (Fig. 3a). Prior studies have indicated that incorporating alloying elements like Cu can effectively decrease the size and quantity of α colonies in the microstructure of L-PBFed CP-Ti. This results in the growth of only a few small colonies at the boundaries of partially melted Ti particles and within the equiaxed prior β grains, as shown in Fig. 3a [6, 28]. By observing Fig. 3b, it is clearly seen that by adding Si to the L-PBFed Ti-5Cu alloy, the length of the α-laths are dramatically reduced. Upon closer examination using a scanning electron microscope (SEM), it is evident from the micrograph in Fig. 3d that certain portions of the lath-shaped α phase have transformed into submicron-sized equiaxed α phase. Si has greatly refined the equiaxed prior β- grains, which in turn severely limit the growth of the lath-like α phase, as illustrated in Fig. 3 d.The distribution histograms and average values of length and width of the lath-like α phase in the microstructure of the L-PBFed Ti-5Cu and the L-PBFed Ti-5Cu-Si samples are given in Fig. 5. It is observed that the average length of α lath has decreased from about 4±0.94 μm in the microstructure of the L-PBFed Ti-5Cu sample (Fig. 5a) to about 1.7±0.6 μm in the microstructure of the L-PBFed Ti-5Cu-Si samples (Fig. 5 b). On the other hand, the histograms illustrating the average length of α-laths show that when Si is introduced to the L-PBFed Ti-5Cu sample, the distribution of average lengths is concentrated within a narrower range and at shorter lengths, as depicted in Fig. 5b. Also, as shown in Fig. 5c and Fig. 5d the average width of the α-laths changed from about 1.1±0.14 μm for the L-PBFed Ti-5Cu sample to about 0.72±0.16 μm for the L-PBFed Ti-5Cu-Si sample.

Prior research has indicated that the primary factors contributing to the reduction in the size of the lath-like α phase and α colonies in the microstructure of Ti6Al4V-xB alloys following boron addition are the growth restriction of refined prior β grains and the enhancement of nucleation rate caused by the discontinuous α_{GB} and TiB phases [33,34].

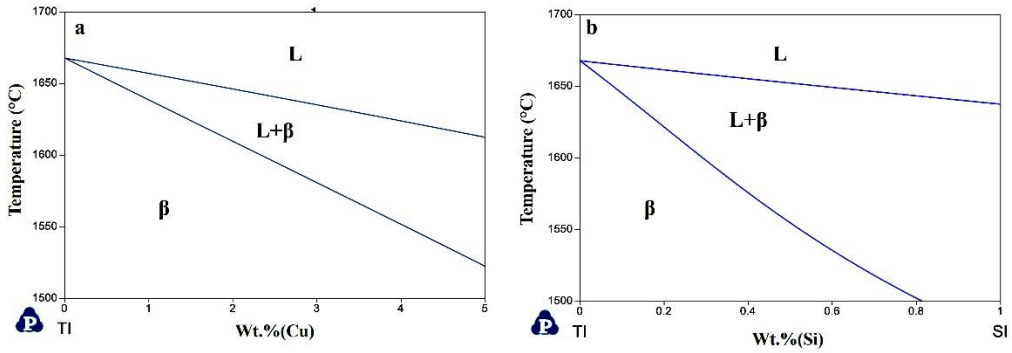

Fig. 4- Low solute content side of the phase diagram of a) Ti-Cu and b) Ti -Si alloy systems calculated using Pandat software.

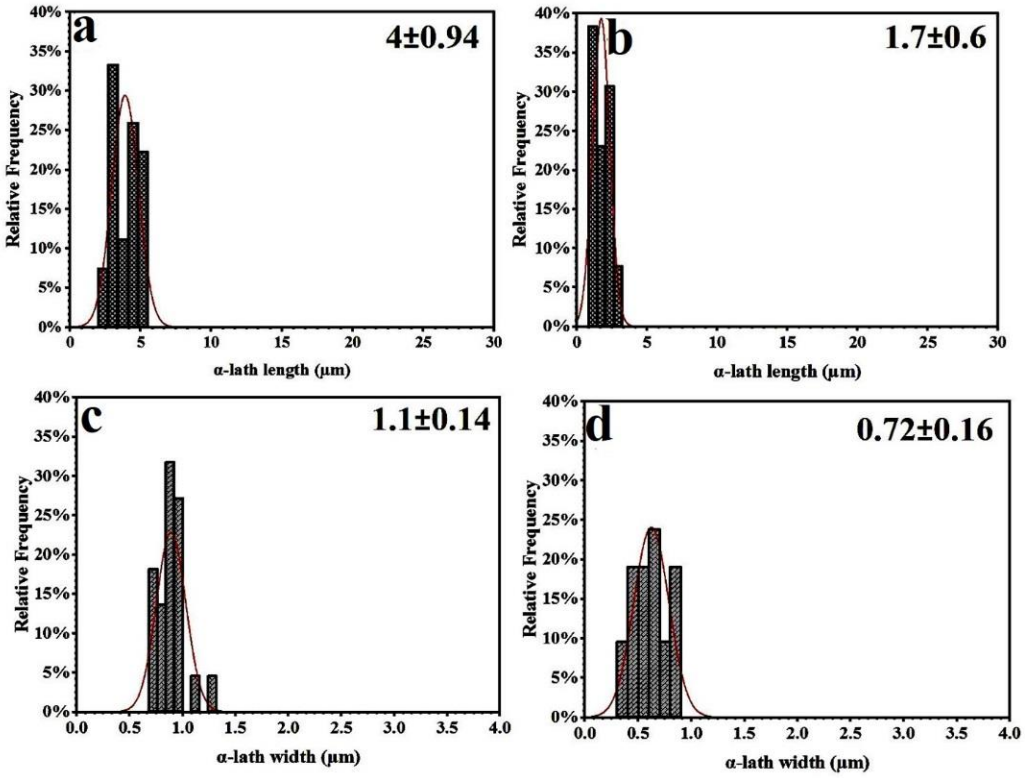

Fig. 5- Distribution histograms and the average value of a,b) length and c,d) width of the α-laths related to the L-PBFed Ti-5Cu and the L-PBFed Ti-5Cu-Si samples, respectively.

3.4 Microstructural homogeneity

3.4.1 Distribution of Cu and Si in L-PBFed Ti-5Cu-1Si microstructure

SEM, FESEM, and EDX methods were utilized to conduct more in-depth analyses on the microstructural homogeneity of Cu and Si distribution in the L-PBFed Ti-5Cu-1Si bulk. Cu tends to segregate at the bottom of fusion layer boundaries, as evidenced by the chemical inhomogeneity observed in the SEM micrograph shown in Fig. 6a. Dark regions, visible as some Ti-enriched areas, have been formed alongside Cu-rich areas without undergoing any dissolution. When selecting materials for in-situ alloying through L-PBF, if they have significantly different properties such as melting points, laser absorption coefficients, powder particle sizes, thermal conductivity, and various other thermo-physical variances, they often result in the presence of numerous unmelted particles within the microstructure. [15-17]. Yadroitsev et al. [17] reported that due to the lower melting point and smaller particle size of Cu compared to those of Ti, Cu powder particles were fused first during the in-situ alloying of Ti6Al4V-1.38%Cu using L-PBF, and unmelted Ti particles remained. Mosallanejad et al. [16] pointed out that the shallow melt pool formed when a laser interacts with Cu powder particles, as opposed to Ti, is primarily due to copper's high thermal conductivity and low laser absorption coefficient in comparison to Ti. Apart from the complete melting of particles, processes in the molten pool, convection, Marangoni flows, density and viscosity gradients are key factors in determining the homogeneity of an alloy in the in situ alloying approach [15,17].

In fact, Ti and Cu are featured with completely different viscosities and densities. Hence, if in-situ alloying of Ti-Cu-based alloys is conducted with inadequate VED and low heat input the disparity in viscosity between the Cu and Ti molten metals, along with the absence of mass transfer through diffusion, will cause the distribution of Cu -rich regions within a viscous liquid Ti [17,18]. Cu has a higher density compared to Ti. This leads to Cu sinking to the bottom of the molten pool and clustering near the boundaries due to the lack of mass transfer caused by mixing in the viscous Ti alloy melt [17,18]. A new set of manufacturing parameters, such as a higher VED generating a

bigger molten pool, would possibly guarantee a more homogeneous Ti-Cu-based alloy [16-19]. Higher temperatures and longer existence times of a big molten pool than those of a small one, cause mass transfer by diffusional processes and mixing can dissolve more Cu in the Ti matrix. When the melt pool is larger, the cooling rates are lower, and the temperatures are higher. This creates extended periods for Cu to diffuse into the Ti lattice. Additionally, it decreases the viscosity gap between Cu and Ti, promoting increased mass transfer through diffusion and mixing [16-19]. FESEM micrographs with a higher magnification in Fig. 6b shows the formation of Cu and Si-rich regions around partially melted Ti particles. The EDX mapping in Fig. 6c shows the segregation of Cu and Si elements around the Ti-rich regions in the L-PBFed Ti-5Cu-Si microstructure. Partial melting of Ti and its lack of complete dissolution with Cu and Si elements has caused micro segregation of Cu and Si adjacent to Ti -rich areas.

3.4.2 Effect of Cu micro segregation on Ti_2Cu formation

The FESEM image in Fig. 7a and a high magnification micrograph of Fig. 7a (Fig. 7b) shows the formation of a dendritic phase adjacent to an unmelted Ti particle. The EDX point and line analyses conducted on the dendritic phase in Fig. 7c and Fig. 7d revealed that this dendritic phase is rich in Cu with a content of about 38.54 wt.%.

To examine and verify the presence of Cu-rich precipitates near the unmelted Ti particles more thoroughly, we utilized PANDAT software to plot non-equilibrium solidification curves for two alloys: Ti-5 wt% Cu and Ti-14 wt% Cu. The results are shown in Fig. 8a and b. These curves clearly show that the final phase under the rapid cooling conditions of the L-PBF process is the Ti_2Cu phase. Also, XRD measurements were performed to identify the phase formation in the microstructure of the L-PBFed Ti-5Cu-1Si sample. The existence of the low-intensity Ti_2Cu peaks in the L-PBFed Ti-5Cu-1Si XRD pattern (Fig. 9) definitively confirmed the presence of a low content of this phase in the microstructure.

The presence of Ti_2Cu intermetallic precipitates has been reported in pure Ti and Ti alloys by conventional manufacturing methods, namely casting with the addition of Cu between 1-10 wt. % Cu [35,36]. However, according to recent studies, Ti_2Cu precipitates were found to be unavoidable regardless of the cooling rate applied, even in the L-BPF process. Ti_2Cu intermetallic precipitates may appear as a result of repeated thermal cycling during the AM processes, where the material is subjected to multiple heating and cooling cycles with the manufacturing of new layers [10,12]. On the other hand, due to micro segregations and inhomogeneous microstructure within Ti-Cu-based alloys, regions with high Cu content could bring the composition to the eutectoid point presented in the Ti-Cu phase diagram [19]. Also, the authors revealed that the thermal history of L-BPF accumulated heat during the deposition of successive layers, which in turn reduced the cooling rate and $\beta \rightarrow \alpha + Ti_2Cu$ completed before the martensite transformation was reached [10,12].

4. Conclusions

This article presents the results of an investigation on the influence of in-situ alloying with Si on the microstructure of a Ti-5Cu alloy synthesized via L-PBF process. The conclusions are briefly outlined:

- Columnar β grains in the as-built Ti-5Cu microstructure were successfully converted into equiaxed prior β grains in the as-built Ti-5Cu-1Si sample.
- Si addition induced fine equiaxed prior β grains with an average size of 7.6 μm in the as-built Ti-5Cu-1Si microstructure.
- The columnar to equiaxed transition phenomena and formation of finer-sized-equiaxed prior β grains in the microstructures of as- as-built Ti-5Cu-1Si samples were attributed to the significant effect of Si addition on the formation of a constitutional supercooling zone ahead of the columnar β grains solidification front.
- Si addition reduced the length and width of lath-like α phase in as-built Ti-5Cu-1Si microstructure.

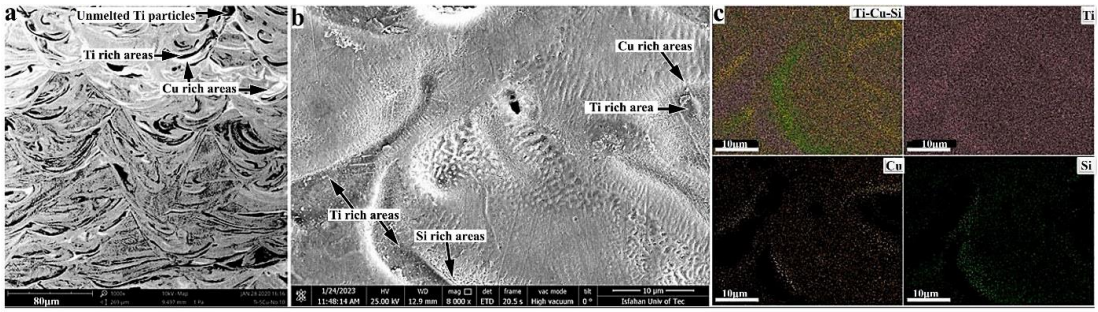

Fig. 6- a) SEM and b) FESEM micrographs of the L-PBFed Ti-5Cu-Si sample along with c) EDX map of Cu, Si and Ti in (b).

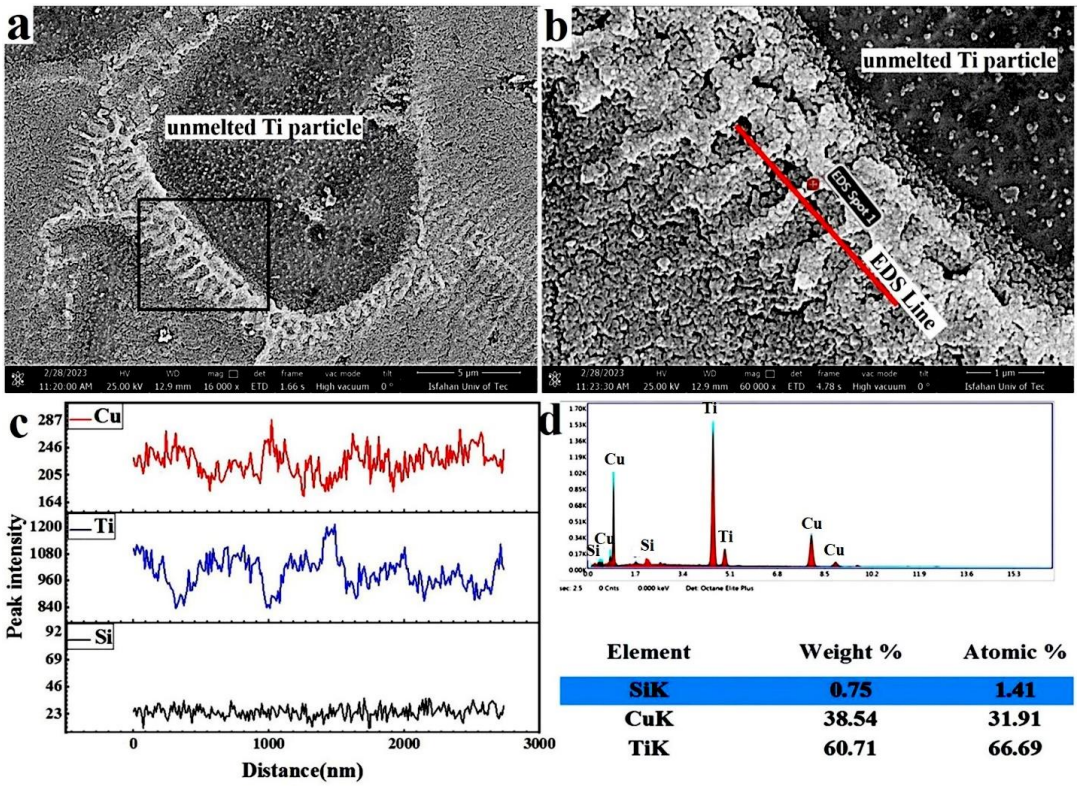

Fig. 7- a) FESEM micrograph of L-PBFed Ti-5Cu-1Si sample, b) higher magnification of (a) showing dendritic Ti2Cu intermetallic phases, c) the EDX line and d) point analyses from dendritic Ti2Cu intermetallic phases.

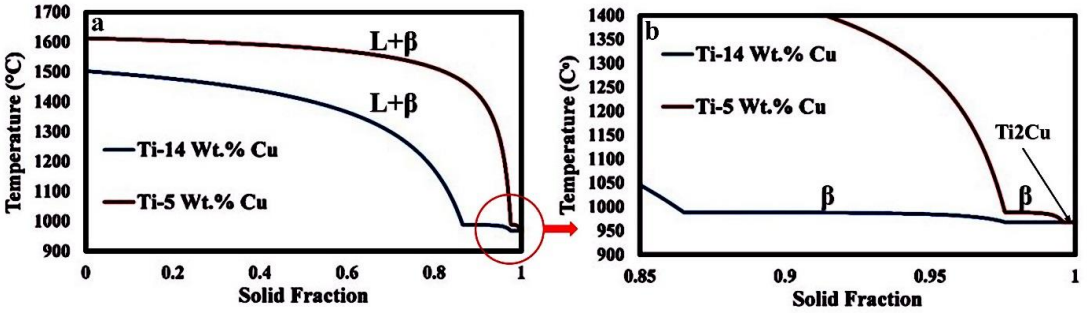

Fig. 8- a, b) Non-equilibrium solidification curves of Ti-5 wt.%.Cu and Ti-14 wt.%. Cu alloys.

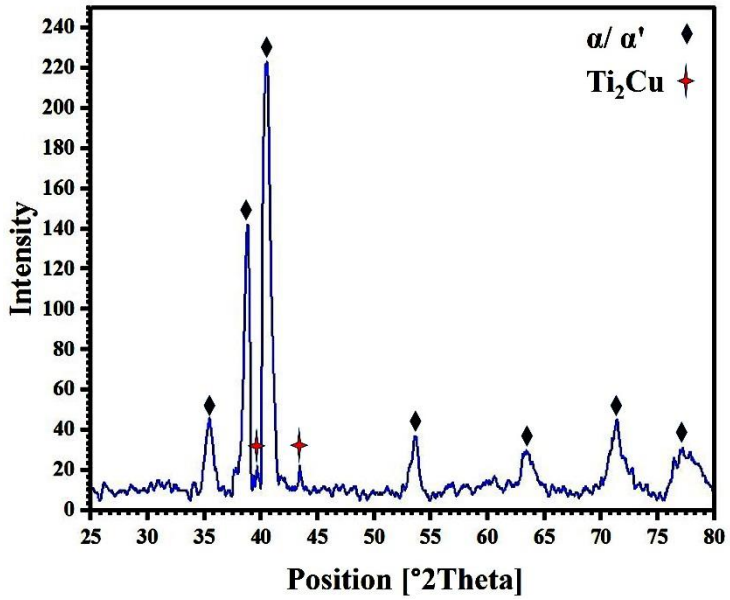

Fig. 8- XRD pattern for L-PBFed Ti-5Cu-1Si sample.

References

1. Herzog. D, Seyda V, Wycisk E, Emmelmann C, Additive Manufacturing of Metals, Acta Mater. 2016; 117 (1): 371–392.
2. Collins PC, Brice DA, Samimi P, Ghamarian I, Fraser HL. Microstructural Control of Additively Manufactured Metallic Materials. Annual Review of Materials Research. 2016;46(1):63-91.
3. M. Dadkhah, M.H. Mosallanejad, L. Iuliano, A. Saboori, A comprehensive overview on the latest progress in the additive manufacturing of metal matrix composites: potential, challenges, and feasible solutions, Acta Metall. Sin. (Engl. Lett. 34 (2021) 1173–1200.
4. M. S. Safavi, A. Azarniya, M. F. Ahmadipour, M. V. Reddy, New-emerging approach for fabrication of near net shape aluminum matrix composites/nanocomposites: Ultrasonic additive manufacturing, Journal of Ultrafine Grained and Nanostructured Materials, 2019;52:188–196.
5. A. Saboori, D. Gallo, S. Biamino, P. Fino, M. Lombardi, An overview of additive manufacturing of titanium components by directed energy deposition: microstructure and mechanical properties, Appl. Sci. (2017).
6. Talebi. M, Niroumand B, Razaghian A, Saboori A, Iuliano L, Process-induced microstructural variations in laser powder bed fusion of novel titanium alloys: A comprehensive study on volumetric energy density and alloying effects, Journal of Materials Research and Technology 2024;31:1430–1442.
7. A. Saboori, A. Abdi, S.A. Fatemi, G. Marchese, S. Biamino, H. Mirzadeh, Hot deformation behavior and flow stress modeling of Ti–6Al–4V alloy produced via electron beam melting additive manufacturing technology in single β-phase field, Mater. Sci. Eng. A 792 (2020), 139822.
8. J. Gholamzadeh, S.M. Fatemi, N. Mollaei, A. Abedi, Processing of Ultrafine/nano-grained microstructures through additive manufacturing techniques: a critical review, Journal of Ultrafine Grained and Nanostructured Materials, 2024;57:203–221.
9. M. J. Bermingham, D. H, StJohn, b. J. Krynen, S. Tedman-Jones, M. S. Dargusch, Promoting the columnar to equiaxed transition and grain refinement of titanium alloys during additive manufacturing, Acta Mater., 168, 2019, 261–274.
10. Zhang D, Qiu D, Gibson MA, Zheng Y, Fraser HL, StJohn DH, Easton MA. Additive manufacturing of ultrafine-grained high-strength titanium alloys. Nature. 2019;576(7785):91-5.
11. Mantri SA, Alam T, Choudhuri D, Yannetta CJ, Mikler CV, Collins PC, Banerjee R. The effect of boron on the grain size and texture in additively manufactured β-Ti alloys. Journal of Materials Science. 2017;52(20):12455-66.
12. Mosallanejad MH, Niroumand B, Ghibaudo C, Biamino S, Salmi A, Fino P, Saboori A. In-situ alloying of a fine grained fully equiaxed Ti-based alloy via electron beam powder bed fusion additive manufacturing process. Additive Manufacturing. 2022;56:102878.
13. Mereddy S, Bermingham MJ, StJohn DH, Dargusch MS. Grain refinement of wire arc additively manufactured titaniumby the addition of silicon. Journal of Alloys and Compounds. 2017;695:2097-103.
14. StJohn DH, Qian M, Easton MA, Cao P. The Interdependence Theory: The relationship between grain formation and nucleant selection. Acta Materialia. 2011;59(12):4907-21.
15. Mosallanejad MH, Niroumand B, Aversa A, Saboori A. In-situ alloying in laser-based additive manufacturing processes: A critical review. Journal of Alloys and Compounds. 2021;872:159567.
16. M.H. Mosallanejad, B. Niroumand, A. Aversa, D. Manfredi, A. Saboori, Laser Powder Bed Fusion in-situ alloying of Ti-5%Cu alloy: process-structure relationships, J. Alloy. Compd. 857 (2021), 157558.
17. Yadroitsev I, Krakhmalev P, Yadroitsava I. Titanium Alloys Manufactured by In Situ Alloying During Laser Powder Bed Fusion. JOM. 2017;69(12):2725-30.
18. Krakhmalev P, Yadroitsev I, Yadroitsava I, de Smidt O. Functionalization of Biomedical Ti6Al4V via In Situ Alloying by Cu during Laser Powder Bed Fusion Manufacturing. Materials (Basel). 2017;10(10):1154.
19. Vilardell AM, Yadroitsev I, Yadroitsava I, Krakhmalev P, Kouprianoff D, Kothleitner G, et al. Manufacturing and characterization of in-situ alloyed Ti6Al4V (ELI)-3 at.% Cu by Laser powder bed fusion. Addit Manuf 2020;36:1–29.
20. C.D. Boley, S.A. Khairallah, A.M. Rubenchik, Calculation of laser absorption by metal powders in additive manufacturing, Appl. Opt. 54 (2015) 2477–2482.
21. J.J. Valencia, P.N. Quested, Thermophysical Properties

Sources and Availability of Reliable Data, ASM, 2008.
22. A. M. Vilardell, A. Takezawa, A. du Plessis, N. Takata, P. Krakhmalev, M. Kobashi, M. Albu, G. Kothleitner, I. Yadroitsava, I. Yadroitsev, Mechanical behavior of in-situ alloyed Ti6Al4V(ELI)-3 at.% Cu lattice structures manufactured by laser powder bed fusion and designed for implant applications, J. Mech. Behav. Biomed. Mater. 113, 2021, 104130.
23. A. M. Vilardell, V. C. Alzamora, L. V. Bauso, C. Madrid, P. Krakhmalev, M. Albu, I. Yadroitsava, I. Yadroitsev, N. G. Giralt, Effect of Heat Treatment on Osteoblast Performance and Bactericidal Behavior of Ti6Al4V(ELI)-3at.%Cu Fabricated by Laser Powder Bed Fusion, J. Func Biomatt, Vol. 14, pp. 2 – 19, 2023.
24. X. Xu, Y. Lu, S. Li, S. Guo, M. He, K. Luo, J. Lin, Copper-modified Ti6Al4V alloy fabricated by selective laser melting with pro-angiogenic and anti-inflammatory properties for potential guided bone regeneration applications, Mater. Sci. Eng. C., 90, 2018, 198–210.
25. Wang X, Chen L Y, Sun H, Zhang L, Corrosion behavior and mechanisms of the heat-treated Ti5Cu produced by laser powder bed fusion, Corrosion Science, 2023; 221: 111336.
26. D. Gu, Y. C. Hagedorn, W. Meiners, G. Meng, R.J.S. Batista, K. Wissenbach, R. Poprawe, Densification behavior, microstructure evolution, and wear performance of selective laser melting processed commercially pure titanium, Acta Mater. 60, 2012, 3849–3860.
27. Li L, Chen Y, Lu Y, Qin S, Huang G, Huang T, Lin J. Effect of heat treatment on the corrosion resistance of selective laser melted Ti6Al4V3Cu alloy. Journal of Materials Research and Technology. 2021;12:904-15.
28. Talebi M, Razaghian A, Saboori A, Niroumand B, Effects of Cu addition and heat treatment on the microstructure and hardness of pure Ti prepared by Selective laser melting (SLM), Journal of Ultrafine Grained and Nanostructured Materials, 2023;56:213–223.
29. Liu S, Shin YC. Additive manufacturing of Ti6Al4V alloy: a review. Mater Des 2019;164:107552.
30. Schmid-Fetzer R, Kozlov A. Thermodynamic aspects of grain growth restriction in multicomponent alloy solidification. Acta Materialia. 2011;59(15):6133-44.
31.M. Sun, D.H. StJohn, M.A. Easton, K. Wang, and J. Ni, Effect of cooling rate on the grain refinement of Mg-Y-Zr alloys, Metall. Mater. Trans. A, Vol. 51, pp. 482 – 496, 2019.
32. B. B. Welk, N. Taylor, J. Wang, K. Kloenne, k. J. Chaput, S. Fox, H. L. Fraser, Use of alloying to effect an equiaxed microstructure in additive manufacturing and subsequent heat treatment of high-strength titanium alloys, Metall. Mater. Trans. A, 52, 2021, 5367–5380.
33. Xue A, Lin X, Wang L, Wang J, Huang W. Influence of trace boron addition on microstructure, tensile properties and their anisotropy of Ti6Al4V fabricated by laser directed energy deposition. Materials & Design. 2019;181:107943.
34. Zhang K, Tian X, Bermingham M, Rao J, Jia Q, Zhu Y, et al. Effects of boron addition on microstructures and mechanical properties of Ti-6Al-4V manufactured by direct laser deposition. Materials & Design. 2019;184:108191.
35. R. Liu, K. Memarzadeh, B. Chang, Y. Zhang, Z. Ma, R.P. Allaker, L. Ren, K. Yang, Antibacterial effect of copper-bearing titanium alloy (Ti-Cu) against Streptococcus mutans and Porphyromonas gingivalis, Sci Rep. 6(2016) 29985.
36. C. Peng, Y. Liu, H. Liu, S. Zhang, C. Bai, Y. Wan, L. Ren, K. Yang, Optimization of annealing treatment and comprehensive properties of Cu-containing Ti6Al4V-xCu alloys, J. Mater. Sci. Technol. 35 (2019) 2121–2131.